ROYAL SOCIETY
OF CHEMISTRY

PAPER

Computational insights into structural, electronic, and optical properties of Janus GeSO monolayer

Thi-Nga Do,[ab] Nguyen N. Hieu, [ID][cd] N. A. Poklonski, [ID][e] Nguyen Thi Thanh Binh,[f] Cuong Q. Nguyen[cd] and Nguyen D. Hien*[g]

Although O is an element of chalcogen group, the study of two-dimensional (2D) O-based Janus dichalcogenides/monochalcogenides, especially their 1T-phase, has not been given sufficient attention. In this work, we systematically investigate the structural, electronic, and optical properties of 1T Janus GeSO monolayer by using the density functional theory. *Via* the analysis of phonon spectrum and evaluation of elastic constants, the GeSO monolayer is confirmed to be dynamically and mechanically stable. Calculated results for the elastic constants demonstrate that the Janus GeSO monolayer is much mechanically flexible than other 2D materials due to its small Young's modulus. At the ground state, while both GeS_2 and GeO_2 monolayers are indirect semiconductors, the Janus GeSO monolayer is found to be a direct band gap semiconductor. Further, effective masses of both electrons and holes are predicted to be directionally isotropic. The Janus GeSO monolayer has a broad absorption spectrum, which is activated from the visible light region and its absorption intensity is very high in the near-ultraviolet region. The calculated results not only systematically provide the fundamental physical properties of GeSO monolayer, but also stimulate scientists to further studying its importance both theoretically and experimentally.

1 Introduction

Two-dimensional (2D) systems have drawn great interest due to their outstanding physical properties.[1,2] After the discovery of graphene in 2004,[3] a series of other 2D materials have been intensively studied by both the theoretical and experimental methods.[4,5] 2D structures of silicene, phosphorene, h-boron nitride, germanane, or transitional metal dichalcogenides (TMDs) have been predicted to be promising candidates for next-generation electronic devices.[6–10]

Janus 2D structure has recently emerged as a novel 2D material which has received widespread attention.[11,12] Especially, breaking the lattice symmetry of Janus monolayer might enable a number of interesting effects. For example, graphene-based Janus structure, graphene formed by selective hydrogen decorations on one side of graphene has been shown theoretically to be ferromagnetic indirect bandgap semiconductor and suitable for UV optoelectronic applications.[13] Isolation of partially hydrogenated single-sided graphene was demonstrated by Haberer *et al.*[14] Following graphene, 2D Janus TMDs have been synthesized successfully and predicted to exhibit many remarkable quantum effects such as Weyl fermions,[15] charge density wave,[16] superconductivity,[16] and novel excitonic and valleytronic phenomena.[12,17–20]

The out-of-plane asymmetric structure in Janus materials has been observed experimentally.[11] Due to the lacking of mirror symmetry, Janus 2D-TMCs exhibit numerous exotic physical properties associated with wide-ranging electronic properties from metallic to semiconducting and even superconducting, making them potential candidate for various applications such as optoelectronics, spintronics and valleytronics.[21–23] The evolving of the Janus monolayer structure from TMD by completely replacing one layer of chalcogen atoms by another group-VI element leads to asymmetric dipole distribution, which results in a "colossal vertical electric field" within the monolayer of the Janus structure and consequently opens up their new application fields.[24,25] Beside the Janus structures of TMDs, Janus monochalcogenides have also been of great interest in recent years.[26,27] Guo and co-worked demonstrated that the Janus group III monochalcogenides have much higher piezoelectric coefficients than that of the corresponding group-III monochalcogenide monolayers.[28] These Janus structures

*a*Laboratory of Magnetism and Magnetic Materials, Advanced Institute of Materials Science, Ton Duc Thang University, Ho Chi Minh City, Vietnam. E-mail: dothinga@tdtu.edu.vn

*b*Faculty of Applied Sciences, Ton Duc Thang University, Ho Chi Minh City, Vietnam

*c*Institute of Research and Development, Duy Tan University, Da Nang 550000, Vietnam. E-mail: hieunn@duytan.edu.vn

*d*Faculty of Environmental and Natural Sciences, Duy Tan University, Da Nang 550000, Vietnam

*e*Faculty of Physics, Belarusian State University, Minsk 220030, Belarus

*f*Faculty of Fundamental Sciences, Quang Binh University, Quang Binh, Vietnam

*g*Institute of Applied Technology, Thu Dau Mot University, Binh Duong Province 75000, Vietnam. E-mail: nguyendinhhien@tdmu.edu.vn

have also been proven to have efficient photocatalytic performance.[26] Janus group-III monochalcogenide XGaInY (X, Y = S, Se, and Te) monolayers show strong light absorption coefficients ($>10^4$ cm^{-1}) in the visible and ultraviolet regions and suitable band edge positions for water splitting.[29] Another novel family of Janus structures, GaInX$_2$ (X = S, Se), present an external electric field tunable band and band edge positions, turning them into promising candidates in photocatalysis.[30]

Currently, Janus 2D materials based on group-IV dichalcogenides are studied thoroughly by different groups. In particular, Janus structure dichalcogenide monolayer of IV-group GeSSe is predicted with a high piezoelectric coefficient, small Young's modulus, and semiconducting nature, promising futuristic applications in energy harvesting, nanopiezoelectric field-effect transistors, atomically thin sensors, shear/torsion actuators, transducers, self-powered circuits in nanorobotics, electromechanical memory devices, biomedical, and other nanoelectronic applications.[31] It is well known that oxygen exhibits a prominent electronegativity compared to other chalcogens. Such a characteristic might lead to a number of interesting physical properties in the MOX (M = Ge, Sn; X = S, Se, Te) Janus 2D materials. Recently, GeS$_2$ monolayer has been found to be dynamically stable and show indirect semiconducting characteristics.[31] Moreover, dynamical stability of T-GeO$_2$ (in tetrahedral configuration) monolayer has been predicted by first-principle calculations.[32] The thin layers of GeO$_2$ has also been fabricated.[33,34] Particularly, oxygenation of TMDs or monochalcogenides can create the O-based Janus structures, which have been theoretically demonstrated to display various novel physical properties.[35–37]

In this study, we investigate the structural, electronic, and optical properties of Janus GeSO monolayer by using the density functional theory. First, we will evaluate the relaxed structure of the GeSO monolayer and its dynamical and mechanical stabilities. The extraordinary electronic properties will be next considered. Finally, the unconventional optical response associated with the electronic structure will be explored.

2 Computational details

The calculations were performed within the density functional theory (DFT) implemented in the Quantum Espresso package.[38] The projector augmented wave potentials are used for the DFT calculations to treat the interactions between the valence electrons and the core.[39] The Perdew–Burke–Ernzerhof (PBE) functional in the generalized gradient approximation (GGA) is used to describe the exchange–correlation interaction. To describe accurately the electronic bands with the possible strong electron correlations, the Heyd–Scuseria–Ernzerhof functional (HSE06) is also used in the present work.[40] The Grimme's DFT-D2 approach[41] is performed to treat the long-range weak van der Waals interactions in the Janus material. The kinetic energy cutoff is set to be 500 eV for the plane waves included in the basis set and the force-convergence criterion is to be 0.001 eV Å^{-1}. To eliminate any interactions between neighbor plates, we fix the vacuum space along the z direction being 20 Å. The Γ-centered k-point meshes of 15 × 15 × 1 were generated based
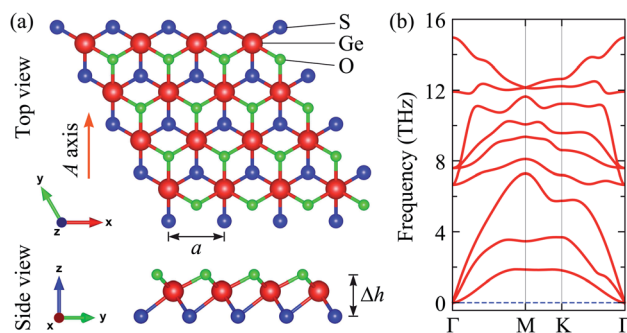

Fig. 1 Optimized structure (a) and phonon spectrum (b) of the Janus GeSO monolayer. Red, blue, and green balls refer to the Ge, S, and O atoms, respectively. *A* axis is the axis along the armchair direction.

on the Monkhorst–Pack scheme[42] for the structural relaxation and evaluation of the electronic properties. The phonon dispersion curves are calculated by using density-functional perturbation theory (DFPT)[43] based on the Quantum Espresso code.[38] A large supercell of 6 × 6 × 1 was used for the phonon spectrum calculations to obtain accurate results.

3 Results and discussion

3.1 Atomic structure and stability

The structure of the studied 2D materials can exist in several kinds of atomic crystal, including 2H and 1T, 1T′, and 3R structural phases.[44] The 1T Janus GeSO monolayer can be constructed from 1T GeS$_2$ or GeO$_2$ monolayers. By replacing the top layer of S atoms with O atom, the 1T Janus GeSO can be built as shown Fig. 1(a). While the hexagonal structures of GeS$_2$ and SnO$_2$ monolayers belong to the $P\bar{3}m1$ group, the 1T Janus GeSO monolayer belongs to the $P3m1$ space group. Due to the lack of mirror symmetry, the symmetry of the Janus GeSO monolayer is lower than that of GeS$_2$ or GeO$_2$ monolayer. The vertical asymmetry in GeSO is clearly seen through the large difference in bond lengths between Ge–S and Ge–O bonds. The Ge–S and Ge–O bond lengths are calculated to be 2.33 and 2.07 Å, respectively. Our calculated results demonstrated that the optimized lattice constant of the Janus GeSO is 3.19 Å, which is between the values of GeS$_2$ (3.44 Å) and GeO$_2$ (2.90 Å). The calculated structural parameters of 1T GeS$_2$, GeO$_2$, and GeSO monolayers are listed in Table 1.

To examine the dynamical stability, we calculate the phonon dispersion of the Janus GeSO monolayer as presented in Fig. 1(b). The dynamical stability of materials can be evaluated

Table 1 Optimized lattice constant a (Å), the bond length d (Å), buckling constant Δh (Å), and bond angle ϕ (deg) of Janus GeSO monolayer

	a	$d_{\text{Ge–S}}$	$d_{\text{Ge–O}}$	Δh	$\phi_{\angle \text{SGeS}}$	$\phi_{\angle \text{OGeO}}$	$\phi_{\angle \text{OGeS}}$
GeS$_2$	3.44	2.43	—	2.79	89.73	—	—
GeO$_2$	2.90	—	1.94	1.95	—	83.04	—
GeSO	3.19	2.33	2.07	2.36	—	—	88.61

via the analysis of their vibrational spectra. The stability of materials is confirmed if there are no imaginary frequencies in its phonon curves. The primitive cell of GeSO contains three atoms, therefore, its phonon spectrum has nine vibrational modes. Three acoustic modes are observed in the low-frequency region and six optical modes are in the higher frequencies. From Fig. 1(b), we can see that there is no gap between the acoustic and optical phonon branches. This leads to the strong acoustic-optical scattering in the GeSO monolayer, which may affect its thermal conductivity. More importantly, there are no imaginary frequencies in the phonon spectrum, suggesting that the Janus GeSO is dynamically stable and one can experimentally synthesis it as a free-standing monolayer.

Further, the mechanical stability of the Janus GeSO monolayer is tested by calculating their elastic constants C_{ij}. The elastic constants are key parameters that are directly related to the mechanical stability as well as the elastic properties of the material. As denoted by the Voigt notation, there are four independent elastic constants: C_{11}, C_{22}, C_{12}, and C_{66}. The angular-dependence of in-plane stiffness or 2D Young's modulus $Y_{2D}(\theta)$ and Poisson's ratio $\nu(\theta)$ can be written as the following[31]

$$Y_{2D}(\theta) = \frac{C_{11}C_{22} - C_{12}{}^2}{C_{11}A^4 + C_{22}B^4 + A^2B^2\left(\dfrac{C_{11}C_{22} - C_{12}{}^2}{C_{66}} - 2C_{12}\right)}, \quad (1)$$

$$\nu(\theta) = \frac{C_{12}(A^4 + B^4) - A^2B^2\left(C_{11} + C_{22} - \dfrac{C_{11}C_{22} - C_{12}{}^2}{C_{66}}\right)}{C_{11}A^4 + C_{22}B^4 + A^2B^2\left(\dfrac{C_{11}C_{22} - C_{12}{}^2}{C_{66}} - 2C_{12}\right)}, \quad (2)$$

where $A = \sin\theta$ and $B = \cos\theta$ with θ is the polar angle relative to the armchair axis (A axis in Fig. 1).

The Janus GeSO monolayer, as shown in Fig. 1, has hexagonal structure. Hence, we have $C_{11} = C_{22}$ and the C_{66} can be obtained by expression $C_{66} = (C_{11} - C_{12})/2$. Therefore, there are only two independent elastic constants C_{11} and C_{12} needed. The Y_{2D}, ν and 2D shear modulus G_{2D} along the x or y direction for GeSO can be written as follows[45]

$$Y_{2D} = (C_{11}{}^2 - C_{12}{}^2)/C11; \quad G_{2D} = C_{66}; \quad \nu = C_{12}/C_{11}. \quad (3)$$

Obtained results for the elastic constants of GeS$_2$, GeO$_2$, and GeSO monolayers are listed in Table 2. The elastic constants of GeSO are calculated to be $C_{11} = 88.16$ N m^{-1} and $C_{12} = 49.90$ N m^{-1}. The C_{11} of GeSO is smaller than that of both GeS$_2$ and GeO$_2$, while the Janus GeSO has higher C_{12} compared with GeS$_2$

and GeO$_2$. Importantly, the elastic constants of all three monolayers satisfy the Born criteria for mechanical stability[46] that $C_{11} > 0$ and $C_{11}{}^2 - C_{12}{}^2 > 0$. It implies that these monolayers are mechanically stable. Our estimated Young's modulus of the Janus GeSO is 59.90 N m^{-1}, which is comparable with that of Janus SnSSe monolayer (57.50 N m^{-1}).[47] We can see that the GeSO monolayer has a low in-plane stiffness compared to that of other 2D materials, such as MoS$_2$ (130 N m^{-1}),[48] 2D haeckelites ($\sim$300 N m^{-1}),[49] 2D ruthenium carbide (70.38 N m^{-1}),[50] 2D PC$_3$ (190 N m^{-1}),[51] and boron-carbon-nitride (291 N m^{-1}).[52] This suggests that the Janus GeSO monolayer is more flexible than those 2D structures and can withstand applied strain in large elongation. In Fig. 2, the angle-dependence of Young's modulus and Poisson's ratio of all three monolayers is illustrated in the polar diagram plot. Our calculated results demonstrate that the $Y_{2D}(\theta)$ and $\nu(\theta)$ in the polar diagram have a perfectly circular shape, suggesting that all monolayers GeS$_2$, GeO$_2$, and GeSO possess fully isotropic elastic properties. It is noted that most synthesized 2D structures possess hexagonal symmetry, therefore, they exhibit isotropic in-plane elastic properties.

3.2 Electronic properties

Next, we investigate the electronic properties of the Janus GeSO monolayer. To improve the reliability of our calculation method, we first evaluate the band structure of the 1T-phase of pristine dichalcogenide monolayer GeS$_2$. Our calculated results demonstrate that at the ground state, the GeS$_2$ monolayer is an indirect semiconductor with a band gap of 0.74 eV at the PBE

Fig. 2 Polar diagram for the Young's modulus $Y_{2D}(\theta)$ and Poisson's ratio $\nu(\theta)$ of the Janus GeSO monolayer. θ is the angle relative to the A axis in Fig. 1.
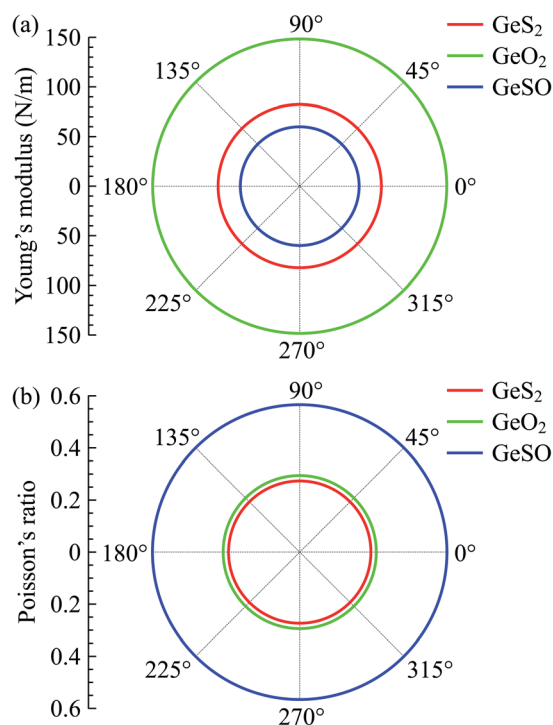
Table 2 Calculated results for elastic constants C_{ij}, Young's modulus Y_{2D}, and Poisson's ratio ν of GeS$_2$, GeO$_2$, and Janus GeSO monolayers

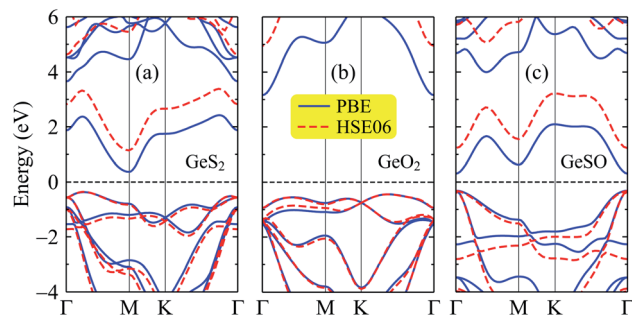|	C_{11} (N m^{-1})	C_{12} (N m^{-1})	C_{66} (N m^{-1})	Y_{2D} (N m^{-1})	ν
GeS$_2$	89.04	24.36	32.34	82.37	0.27
GeO$_2$	162.44	47.80	57.32	148.37	0.29
GeSO	88.16	49.90	19.13	59.90	0.57

Fig. 3 Electron band structures $E(k)$ of GeS$_2$ (a), GeO$_2$ (b), and GeSO (c) monolayers calculated at the PBE and HSE06 levels in the first Brillouin zone.

level. To correct the band gap, the HSE06 hybrid functional was used to evaluate the band structure of GeS$_2$. The band gap of GeS$_2$ is found to be 1.50 eV at the HSE06 level. Our calculated results are good in agreement with the available data (0.73/1.51 eV at the PBE/HSE06 level), which were very recently reported by Nandi and co-workers.[31] This confirms that our computational method for electronic properties is valid. The calculated band structures of GeS$_2$, GeO$_2$, and GeSO monolayers are depicted in Fig. 3. It is seen that while both GeS$_2$ and GeO$_2$ monolayers are indirect semiconductors, the Janus GeSO monolayer exhibits direct semiconducting characteristics with both the conduction band minimum (CBM) and valence band maximum (VBM) located at the Γ symmetry point. There is a large difference in the calculated band gaps by the PBE and HSE06 methods. However, the evaluated band structures at the PBE and HSE06 levels are almost the same profiles as illustrated in Fig. 3. The band gap of the Janus GeSO monolayer is found to be 0.63 and 1.55 eV at the PBE and HSE06 levels, respectively. The band gap of GeSO is close to that of GeS$_2$ but much smaller than that of GeO$_2$ as listed in Table 1. The band gaps of the monolayers are also shown in Fig. 4 for comparison.

To get insights into the formation of the electronic bands, especially the CBM and VBM, we show our evaluated weighted bands of the Janus GeSO in Fig. 5. It is found that the VBM is
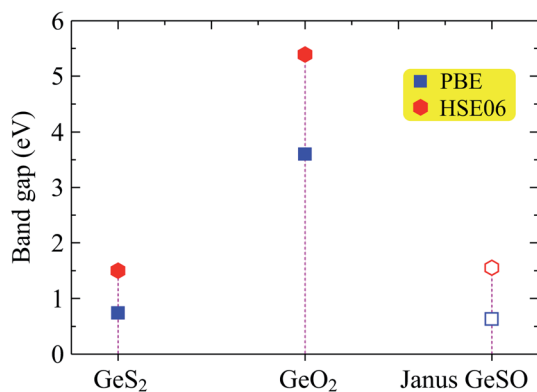

Fig. 4 Calculated band gaps of GeS$_2$, GeO$_2$, and GeSO by using PBE and HSE06 functionals. Filled and opened sharps refer to the indirect and direct gaps, respectively.
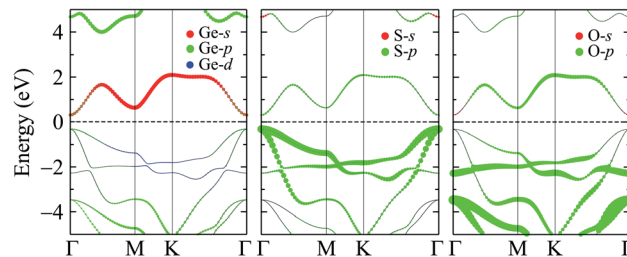

Fig. 5 Calculated weighted bands of the Janus GeSO monolayer using the PBE functional.

mainly contributed by the S-p orbital, while the Ge-s and Ge-p orbitals significantly contribute to the CBM of the Janus GeSO monolayer. In the higher energy regions, the O-p orbitals significantly contribute to both the valence and conduction bands.

Moreover, we calculate the effective masses of the mobile carriers, which are also the key parameters of the materials. The effective masses of electron (m_e^*) and hole (m_h^*) can be obtained by fitting parabolic function to the VBM and CBM through the formula as:

$$\frac{1}{m^*} = \frac{1}{\hbar^2} \left| \frac{\partial^2 E(k)}{\partial k^2} \right|, \qquad (4)$$

where $E(k)$ is the wave-number k-dependent energy (in $k_x k_y$ plane) at the VBM/CBM and $\hbar = h/2\pi$ is the reduced Plank constant. The value of the effective mass depends strongly on the shape of the band structure around the band edges. It is seen that the flatter the band structures around the band edges, the larger the effective masses. The radius of the curve is largely due to the flat band, leading to a small second derivative $\partial^2 E(k)/\partial k^2$ or large effective mass as shown in eqn (4). It is indicated that, at the CBM, the effective masses of electrons m_e^* of GeSO is directionally isotropic along the x and y directions. m_e^* along the $k_x \| x$ and $k_y \| y$ directions of GeSO is calculated to be $0.32 m_0$ with m_0 being the free electron mass. The small effective mass suggests that the carrier responds more quickly to the external field, leading to the high mobility of the carrier. Similarly, at the VBM, the lateral hole effective masses m_h^* along the $k_x \| x$ and $k_y \| y$ directions are $1.24 m_0$ and $1.28 m_0$, respectively. These values suggest that the effective masses of both electrons and holes are directionally isotropic. This is due to the symmetry of the bands around the Γ symmetry point as depicted in Fig. 3(c).

Table 3 Calculated band gap E_g using the PBE and HSE06 methods and effective masses of electron m_e^* and hole m_h^* along the $x \| k_x$ and $y \| k_y$ directions of GeS$_2$, GeO$_2$, and GeSO monolayers

	E_g (eV)		m_e^* (m_0)		m_h^* (m_0)		
	PBE	HSE06	x	y	x	y	Status
GeS$_2$	0.74	1.50	0.42	0.21	0.53	0.63	Indirect
GeO$_2$	3.60	5.40	0.35	0.35	4.45	3.82	Indirect
GeSO	0.63	1.55	0.32	0.32	1.24	1.28	Direct

Compared with the GeS_2 and GeO_2 monolayers, as listed in Table 3, we can see that the carrier effective masses of GeS_2 are directionally anisotropic. Meanwhile, for GeO_2 monolayer, the effective mass of holes is directionally anisotropic and higher than that of electrons. This is due to the flat band around the VBM of GeO_2 as depicted in Fig. 3(b).

3.3 Optical properties

Finally, we study the optical response of the Janus GeSO monolayer. The fundamental optical characteristics of the materials can be evaluated through the frequency-dependent complex dimensionless dielectric function, which is expressed as $\varepsilon(\omega) = \varepsilon_1(\omega) + i\varepsilon_2(\omega)$. The imaginary part of the dielectric function $\varepsilon_2(\omega)$ can be calculated as follows[53]

$$\varepsilon_2^{ij}(\omega) = \frac{4\pi^2 e^2}{Vm^2\omega^2} \sum_{knn'\sigma} \langle kn\sigma|p_i|kn'\sigma\rangle\langle kn'\sigma|p_j|kn\sigma\rangle$$
$$\times f_{kn}(1 - f_{kn'})\delta(E_{kn'} - E_{kn} - \hbar\omega), \quad (5)$$

where e is the elementary charge; $m = m_0$ refers to the free electron mass; V stands for the unit-cell volume; ω is the angular frequency; $|kn\sigma\rangle$ is the wave-function of the crystal with the momentum operator p, and f_{kn} refers to the Fermi distribution function. Then, the real part $\varepsilon_1(\omega)$ can be obtained by using the Kramers–Kronig transformation.[54]

The absorption coefficient $A(\omega)$ is given by[55]

$$A(\omega) = \frac{\sqrt{2}\omega}{c}\left[\sqrt{\varepsilon_1(\omega)^2 + \varepsilon_2(\omega)^2} - \varepsilon_1(\omega)\right]^{1/2}, \quad (6)$$

where c is the speed of light in vacuum.

In this work, the dielectric function $\varepsilon(\omega)$ and absorption coefficient $A(\omega)$ of GeSO are evaluated along the x-direction by HSE06 method. The HSE06 method is investigated as a method that can give accurate results in calculations for optical characteristics of 2D materials.[36,56] The $\varepsilon(\omega)$ and $A(\omega)$ of the Janus GeSO monolayer are illustrated in Fig. 6. It is noted that the static dielectric constant $\varepsilon_1(0)$ is inversely proportional to the direct bandgap of the semiconductor as described by the Penn model.[57] The $\varepsilon_1(0)$ of the Janus GeSO monolayer is 1.99, which is smaller than that of the Janus SnSSe monolayer.[47] As shown in Fig. 6, we can see that the absorption spectrum of the GeSO monolayer is activated in the visible light region (at 1.62 eV) which is consistent with its direct band gap at the HSE06 level. The first peak in the absorption spectrum is located at 3.69 eV as shown in Fig. 6(b). It is demonstrated that GeSO exhibits high absorption intensity in the ultraviolet region, around 9 eV. The maximum absorption coefficient of GeSO calculated by eqn (6) is 8.75×10^5 cm^{-1} at the photon energy of $\hbar\omega = 9.78$ eV.

4 Conclusion

In conclusion, we investigated the fundamental properties of the Janus GeSO by using the DFT calculations. Based on the analysis of phonon spectrum and elastic constants, it is found that the Janus GeSO monolayer is dynamically and mechanically stable at the ground state. The calculated results demonstrated that, with small elastic constants, the GeSO monolayer is more flexible than other 2D materials and that it can withstand the large-amplitude strain and is easily rolled to form nanotubes. The Janus GeSO is predicted to be the indirect semiconductor with a band gap being 0.63 and 1.55 eV at the PBE and HSE06 levels, respectively. We also explore the optical response of the Janus GeSO monolayer, which is calculated to be high absorption intensity in the ultraviolet region. Our findings not only systematically get insights into the physical properties of GeSO monolayer but also creates an important premise for further studies, especially creating a theoretical basis for the prospect of successfully synthesizing GeSO monolayer by experiment.

Conflicts of interest

There are no conflicts to declare.

Acknowledgements

References

1 N. A. Poklonski, S. A. Vyrko, A. I. Siahlo, O. N. Poklonskaya, S. V. Ratkevich, N. N. Hieu and A. A. Kocherzhenko, *Mater. Res. Express*, 2019, **6**, 042002.

2 A. I. Siahlo, N. A. Poklonski, A. V. Lebedev, I. V. Lebedeva, A. M. Popov, S. A. Vyrko, A. A. Knizhnik and Y. E. Lozovik, *Phys. Rev. Mater.*, 2018, **2**, 036001.

3 K. S. Novoselov, A. K. Geim, S. V. Morozov, D. Jiang, Y. Zhang, S. V. Dubonos, I. V. Grigorieva and A. A. Firsov, *Science*, 2004, **306**, 666.

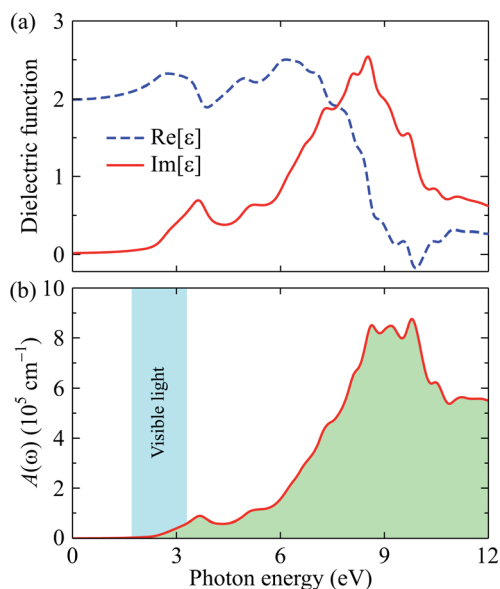

Fig. 6 (a) Dielectric function $\varepsilon(\omega)$ and (b) optical absorption coefficient $A(\omega)$ of GeSO at the ground state. "Re" and "Im" in (a) refer to the real and imaginary parts of the dielectric function, respectively.

4 D. Muoi, N. N. Hieu, C. V. Nguyen, B. D. Hoi, H. V. Nguyen, N. D. Hien, N. A. Poklonski, S. S. Kubakaddi and H. V. Phuc, *Phys. Rev. B*, 2020, **101**, 205408.

5 A. V. Lebedev, I. V. Lebedeva, A. M. Popov, A. A. Knizhnik, N. A. Poklonski and S. A. Vyrko, *Phys. Rev. B*, 2020, **102**, 045418.

6 J. Zhuang, X. Xu, H. Feng, Z. Li, X. Wang and Y. Du, *Sci. Bull.*, 2015, **60**, 1551.

7 A. Carvalho, M. Wang, X. Zhu, A. S. Rodin, H. Su and A. H. Castro Neto, *Nat. Rev. Mater.*, 2016, **1**, 16061.

8 K. Zhang, Y. Feng, F. Wang, Z. Yang and J. Wang, *J. Mater. Chem. C*, 2017, **5**, 11992.

9 A. Acun, L. Zhang, P. Bampoulis, M. Farmanbar, A. van Houselt, A. N. Rudenko, M. Lingenfelder, G. Brocks, B. Poelsema, M. I. Katsnelson and H. J. W. Zandvliet, *J. Phys.: Condens. Matter*, 2015, **27**, 443002.

10 S. Manzeli, D. Ovchinnikov, D. Pasquier, O. V. Yazyev and A. Kis, *Nat. Rev. Mater.*, 2017, **2**, 17033.

11 A.-Y. Lu, H. Zhu, J. Xiao, C.-P. Chuu, Y. Han, M.-H. Chiu, C.-C. Cheng, C.-W. Yang, K.-H. Wei, Y. Yang, Y. Wang, D. Sokaras, D. Nordlund, P. Yang, D. A. Muller, M.-Y. Chou, X. Zhang and L.-J. Li, *Nat. Nanotechnol.*, 2017, **12**, 744.

12 M. Yagmurcukardes, Y. Qin, S. Ozen, M. Sayyad, F. M. Peeters, S. Tongay and H. Sahin, *Appl. Phys. Rev.*, 2020, **7**, 011311.

13 J. Zhou, Q. Wang, Q. Sun, X. S. Chen, Y. Kawazoe and P. Jena, *Nano Lett.*, 2009, **9**, 3867.

14 D. Haberer, C. E. Giusca, Y. Wang, H. Sachdev, A. V. Fedorov, M. Farjam, S. A. Jafari, D. V. Vyalikh, D. Usachov, X. Liu, U. Treske, M. Grobosch, O. Vilkov, V. K. Adamchuk, S. Irle, S. R. P. Silva, M. Knupfer, B. Büchner and A. Grüneis, *Adv. Mater.*, 2011, **23**, 4497.

15 J. Jiang, Z. Liu, Y. Sun, H. Yang, C. Rajamathi, Y. Qi, L. Yang, C. Chen, H. Peng, C.-C. Hwang, S. Sun, S.-K. Mo, I. Vobornik, J. Fujii, S. Parkin, C. Felser, B. Yan and Y. Chen, *Nat. Commun.*, 2017, **8**, 13973.

16 A. H. Castro Neto, *Phys. Rev. Lett.*, 2001, **86**, 4382.

17 J. R. Schaibley, H. Yu, G. Clark, P. Rivera, J. S. Ross, K. L. Seyler, W. Yao and X. Xu, *Nat. Rev. Mater.*, 2016, **1**, 16055.

18 M. Adhib Ulil Absor, H. Kotaka, F. Ishii and M. Saito, *Jpn. J. Appl. Phys.*, 2018, **57**, 04FP01.

19 R. Peng, Y. Ma, S. Zhang, B. Huang and Y. Dai, *J. Phys. Chem. Lett.*, 2018, **9**, 3612.

20 B. Radisavljevic, A. Radenovic, J. Brivio, V. Giacometti and A. Kis, *Nat. Nanotechnol.*, 2011, **6**, 147.

21 K. F. Mak, C. Lee, J. Hone, J. Shan and T. F. Heinz, *Phys. Rev. Lett.*, 2010, **105**, 136805.

22 X. Xu, W. Yao, D. Xiao and T. F. Heinz, *Nat. Phys.*, 2014, **10**, 343.

23 K. F. Mak, K. He, J. Shan and T. F. Heinz, *Nat. Nanotechnol.*, 2012, **7**, 494.

24 L. Dong, J. Lou and V. B. Shenoy, *ACS Nano*, 2017, **11**, 8242.

25 C. Zhang, Y. Nie, S. Sanvito and A. Du, *Nano Lett.*, 2019, **19**, 1366.

26 A. Huang, W. Shi and Z. Wang, *J. Phys. Chem. C*, 2019, **123**, 11388.

27 T. V. Vu, V. T. T. Vi, H. V. Phuc, C. V. Nguyen, N. A. Poklonski, C. A. Duque, D. P. Rai, B. D. Hoi and N. N. Hieu, *J. Phys.: Condens. Matter*, 2021, **33**, 225503.

28 Y. Guo, S. Zhou, Y. Bai and J. Zhao, *Appl. Phys. Lett.*, 2017, **110**, 163102.

29 I. Ahmad, I. Shahid, A. Ali, L. Gao and J. Cai, *RSC Adv.*, 2021, **11**, 17230.

30 H. Yang, P. Zhao, Y. Ma, X. Lv, B. Huang and Y. Dai, *J. Phys. D: Appl. Phys.*, 2019, **52**, 455303.

31 P. Nandi, A. Rawat, R. Ahammed, N. Jena and A. De Sarkar, *Nanoscale*, 2021, **13**, 5460.

32 Y. Guo, S. Zhang, T. Zhao and Q. Wang, *Nanoscale*, 2016, **8**, 10598–10606.

33 K. Okumura, K. Asakura and Y. Iwasawa, *Langmuir*, 1998, **14**, 3607.

34 T. Hibino, M. Niwa, Y. Murakami and M. Sano, *J. Chem. Soc., Faraday Trans. 1*, 1989, **85**, 2327.

35 M. J. Varjovi, M. Yagmurcukardes, F. M. Peeters and E. Durgun, *Phys. Rev. B*, 2021, **103**, 195438.

36 M. Demirtas, B. Ozdemir, Y. Mogulkoc and E. Durgun, *Phys. Rev. B*, 2020, **101**, 075423.

37 T. V. Vu, C. V. Nguyen, H. V. Phuc, A. A. Lavrentyev, O. Y. Khyzhun, N. V. Hieu, M. M. Obeid, D. P. Rai, H. D. Tong and N. N. Hieu, *Phys. Rev. B*, 2021, **103**, 085422.

38 P. Giannozzi, S. Baroni, N. Bonini, M. Calandra, R. Car, C. Cavazzoni, D. Ceresoli, G. L. Chiarotti, M. Cococcioni, I. Dabo, A. Dal Corso, S. de Gironcoli, S. Fabris, G. Fratesi, R. Gebauer, U. Gerstmann, C. Gougoussis, A. Kokalj, M. Lazzeri, L. Martin-Samos, N. Marzari, F. Mauri, R. Mazzarello, S. Paolini, A. Pasquarello, L. Paulatto, C. Sbraccia, S. Scandolo, G. Sclauzero, A. P. Seitsonen, A. Smogunov, P. Umari and R. M. Wentzcovitch, *J. Phys.: Condens. Matter*, 2009, **21**, 395502.

39 G. Kresse and D. Joubert, *Phys. Rev. B: Condens. Matter Mater. Phys.*, 1999, **59**, 1758.

40 J. Heyd, G. E. Scuseria and M. Ernzerhof, *J. Chem. Phys.*, 2003, **118**, 8207.

41 S. Grimme, *J. Comput. Chem.*, 2006, **27**, 1787.

42 H. J. Monkhorst and J. D. Pack, *Phys. Rev. B: Solid State*, 1976, **13**, 5188.

43 T. Sohier, M. Calandra and F. Mauri, *Phys. Rev. B*, 2017, **96**, 075448.

44 S. Das, J. A. Robinson, M. Dubey, H. Terrones and M. Terrones, *Annu. Rev. Mater. Res.*, 2015, **45**, 1.

45 R. C. Andrew, R. E. Mapasha, A. M. Ukpong and N. Chetty, *Phys. Rev. B: Condens. Matter Mater. Phys.*, 2012, **85**, 125428.

46 F. Mouhat and F.-X. Coudert, *Phys. Rev. B: Condens. Matter Mater. Phys.*, 2014, **90**, 224104.

47 S.-D. Guo, X.-S. Guo, R.-Y. Han and Y. Deng, *Phys. Chem. Chem. Phys.*, 2019, **21**, 24620.

48 R. C. Cooper, C. Lee, C. A. Marianetti, X. Wei, J. Hone and J. W. Kysar, *Phys. Rev. B: Condens. Matter Mater. Phys.*, 2013, **87**, 035423.

49 S. Thomas, H. Jung, S. Kim, B. Jun, C. H. Lee and S. U. Lee, *Carbon*, 2019, **148**, 344.

50 S. Thomas and M. A. Zaeem, *Appl. Surf. Sci.*, 2021, **563**, 150232.

51 S. Jana, S. Thomas, C. H. Lee, B. Jun and S. U. Lee, *Carbon*, 2020, **157**, 420.

52 S. Thomas and M. A. Zaeem, *Phys. Chem. Chem. Phys.*, 2020, **22**, 22066.

53 A. Delin, P. Ravindran, O. Eriksson and J. M. Wills, *Int. J. Quantum Chem.*, 1998, **69**, 349.

54 H. Wang, G. Qin, J. Yang, Z. Qin, Y. Yao, Q. Wang and M. Hu, *J. Appl. Phys.*, 2019, **125**, 245104.

55 P. Ravindran, A. Delin, B. Johansson, O. Eriksson and J. M. Wills, *Phys. Rev. B: Condens. Matter Mater. Phys.*, 1999, **59**, 1776.

56 H. L. Zhuang and R. G. Hennig, *Appl. Phys. Lett.*, 2013, **103**, 212102.

57 D. R. Penn, *Phys. Rev.*, 1962, **128**, 2093.